Two-Ray Models in mmWave Communications

Erich Zöchmann*†, Ke Guan‡, and Markus Rupp †
*Christian Doppler Laboratory for Dependable Wireless Connectivity for the Society in Motion
†Institute of Telecommunications, TU Wien, Austria
‡ State Key Laboratory of Rail Traffic Control and Safety, Beijing Jiaotong University, China

***Abstract*—The two-ray model has been used for modelling of wireless channels already for decades. However, since researchers and industry are pushing forward to unlock the millimeter wave bands, we revisited this model. We re-derive the break point distance based on a generalized first Fresnel zone. The simplified approximation formula — four times the product of antenna heights scaled by wavelength — is especially accurate for millimeter waves, but difficult to verify. We then demonstrate that the two-ray ground-reflection model can be observed within many vehicular scenarios and fit ray-tracing data with the two-ray model. Finally we devise a measurement strategy as well as the usage of an ℓ_1 algorithm for piecewise linear fitting slopes to the model data. Thereby we are able to show that the break point distance is indeed a valid modelling parameter and can be determined accurately.**

***Keywords*—break point, mmWave, channel modelling, two-ray model, path loss**

I. Introduction

A. Importance and prior work

The two-ray (2R) model has been used extensively to explain the multi-slope behaviour of observed path loss [1], [2]. It gives a simple to calculate, yet pretty accurate, prediction of receive power. Especially for millimeter waves (mmWave), researchers have observed channels dominated by few specular reflections [3], and therefore, models employing only a few rays are a good choice. The applicability of the 2R model for the current Dedicated Short Range Communication (DSRC) standard around $5.9\,\mathrm{GHz}$ has been shown in [4]–[6]. An extension to the typcial flat surface communcation models has been presented in [7]. The authors of [7] show pathloss models for car-to-car communications on various slope types.

Future vehicular communications could take place at millimeter wave frequencies [8]. The work of [9] used the 2R model for simulations of a joint radar communications system. Evidence for the 2R model can also be found in [10], where the deviations to the 2R model were explained by road undulations. Besides the car-to-car context, the case of train-to-infrastructure communications has been studied experimentally in [11] and through ray-tracing simulations in [12]. Both works show a 2R behaviour. This article will show a fit to the data obtained in [12].

Hand in hand with the 2R model goes the multislope pathloss modeling. For static mmWave scenarios this has already been used in [13], [14]. Peter et al. [15] have been focusing on a methodology to obtain from measurement data (which might obey a 2R model) to proper pathloss coefficient. Our technique for pathloss fitting is built upon [15] and will be based on ℓ_1 trend filtering [16].

B. Our Contributions

We demonstrate on ray-tracing data and on previously conducted measurement campaigns that the two-ray ground-reflection is a suitable small scale fading model for line-of-sight mmWave scenarios. Especially beamforming at least at one link end can be very accurately covered by this model. Closely connected to the two-ray model is the break point distance. The break point distance is used as threshold for an increased pathloss coefficient; thereby being used as large scale fading parameter. Since several expressions for the break point distance exists in the literature, we give a rigorous derivation of the break point distance based on the first (generalized) Fresnel zone. Lastly, we argue that the two-ray model is essentially a small scale fading model. Estimating the break point from a multiple regression model (2 slopes) from the plain observations (measurements or synthetic data) will lead to huge biases. We show a possible preprocessing technique.

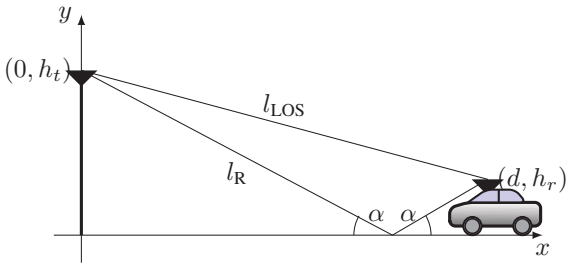

Fig. 1: Two-Ray (Ground-Reflection) model.

II. Review of Two-Ray Ground-Reflection Model

The classical 2R model [2] is a superposition of a signal and a distance dependent delayed copy. Calculating this superposition at exactly one frequency ω, the delay, introduced by the longer ground path, turns into an additional phase. The received magnitude squared of the field strength is given by

$$|E(\omega)|^2 = \left| \frac{E_0 \sqrt{G^t_{\mathrm{LOS}} G^r_{\mathrm{LOS}}}}{l_{\mathrm{LOS}}} e^{-j\frac{\omega}{c} l_{\mathrm{LOS}}} + \Gamma(\alpha,\omega) \frac{E_0 \sqrt{G^t_{\mathrm{R}} G^r_{\mathrm{R}}}}{l_{\mathrm{R}}} e^{-j\frac{\omega}{c} l_{\mathrm{R}}} \right|^2, \tag{1}$$

where E_0 is the transmit field strength, $G^{t/r}_{\mathrm{LOS}}$, $G^{t/r}_{\mathrm{R}}$ are the antenna gains for the transmit antenna and receive antenna in the respective directions, and $\Gamma(\alpha,\omega)$ is the Fresnel reflection coefficient. The distances $l_{\mathrm{LOS}}, l_{\mathrm{R}}$ are sketched in Fig. 1, denote $l_{\mathrm{R}} = l_{\mathrm{LOS}} + \Delta l$. We will assume $d \gg \max(h_t, h_r)$ and therefore $\Gamma(\alpha,\omega) \approx -1$, and $G^t_{\mathrm{LOS}} \approx G^t_{\mathrm{R}}$, $G^r_{\mathrm{LOS}} \approx G^r_{\mathrm{R}}$. Further, the amplitude scaling for both received waves is approximately equal and thereby Equation (1) turns into

$$|E(\omega)|^2 = \frac{E_0^2 G^t G^r}{l^2_{\mathrm{LOS}}} \left| e^{-j\frac{\omega}{c} l_{\mathrm{LOS}}} - e^{-j\frac{\omega}{c}(l_{\mathrm{LOS}}+\Delta l)} \right|^2 \tag{2}$$

$$|E(\omega)|^2 = \frac{E_0^2 G^t G^r}{l^2_{\mathrm{LOS}}} \left(2\sin\left(\frac{2\pi}{\lambda(\omega)} \frac{\Delta l}{2} \right) \right)^2 . \tag{3}$$

Again, due to $d \gg \max(h_t, h_r)$, the path length difference can be approximated to $\Delta l \approx {}^{2h_t h_r}/_{d}$ and $l_{\mathrm{LOS}} \approx d$. The relative

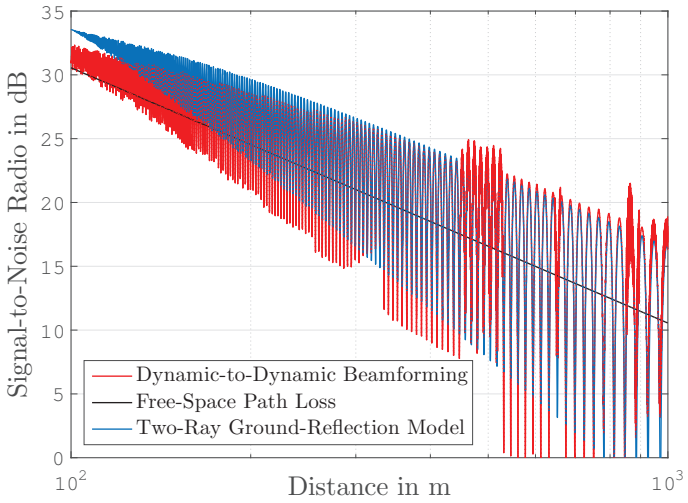

Fig. 2: Signal-to-Noise Ratio (SNR) of a train-to-infrastructure scenario and the corresponding 2R model.

receive power as a function of the geometrical parameters is then given as

$$\frac{P_r}{P_t} = \frac{\lambda^2}{(4\pi d)^2}\left(2\sin\left(\frac{2\pi}{\lambda}\frac{h_t h_r}{d}\right)\right)^2 G^t G^r = L_{2\mathrm{R}} G^t G^r \ . \quad (4)$$

A. Fit with Ray-Tracing Data

The work of [12], has analysed a train-to-infrastructure scenario, where both link ends perform beamforming, thus being entitled dynamic-to-dynamic beamforming, see Fig. 2. The antennas have 25 dBi gain at 100 GHz with 1 GHz bandwidth and use 20 dBm transmit power. The ray-tracing data is modelling an urban area in Beijing. The transmit antenna is mounted in 10 m height and the receiver is on top of the train at 3 m height. Due to the very narrow beams, the reflecting buildings do not impact the results much. The ray-tracing data clearly follows a 2R model.

III. Break Point via Generalized Fresnel Zone

Although not visual in Fig. 2, after a distance called the break point distance d_B, the receive power does not oscillate around the free-space path loss any more and falls off stronger. In this section we prove, that the very simple approximation formula $d_B \approx 4h_t hr/\lambda$, although not easily visible, is still valid for mmWaves.

A. When does a general ellipse touch the ground?

We start with an ellipse where the transmit and receive antenna are in the foci of an ellipse. A reflected signal from any point on the ellipse has the same path length. The parametric form $\boldsymbol{p}(t)$ of an ellipse with parameter $t \in [0, 2\pi)$ and center coordinates (x_c, y_c) can be written as

$$\underbrace{\begin{bmatrix} x(t) \\ y(t) \end{bmatrix}}_{\boldsymbol{p}(t)} = \underbrace{\begin{bmatrix} x_c \\ y_c \end{bmatrix}}_{\boldsymbol{p}_c} + \underbrace{\begin{bmatrix} \cos\varphi & -\sin\varphi \\ \sin\varphi & \cos\varphi \end{bmatrix}}_{\boldsymbol{R}_\varphi} \underbrace{\begin{bmatrix} a & 0 \\ 0 & b \end{bmatrix}}_{\boldsymbol{S}} \underbrace{\begin{bmatrix} \cos t \\ \sin t \end{bmatrix}}_{\boldsymbol{c}(t)} , \quad (5)$$

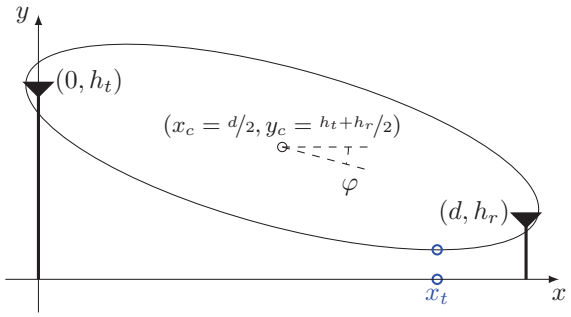

Fig. 3: Ellipse geometry in parametric form.

where φ is the angle between the x-axis and the major axis of the ellipse, see Fig. 3. For our specific problem the following can be stated

$$\boldsymbol{p}_c = \begin{bmatrix} d/2 & (h_t+h_r)/2 \end{bmatrix}^T , \quad -\tan\varphi = (h_t-h_r)/d \ . \quad (6)$$

Thus, an ellipse can be described as affine map of the unit circle $\boldsymbol{c}(t)$, applying a scaling matrix $\boldsymbol{S}$ as well as a rotation matrix $\boldsymbol{R}_\varphi$ onto it.

To obtain the y-axis (ground) touching condition of the ellipse, the y coordinate and its derivative, w.r.t. t, are equated to zero. This gives us the following system of equations

$$\begin{bmatrix} -a\sin\varphi & b\cos\varphi \\ b\cos\varphi & a\sin\varphi \end{bmatrix} \begin{bmatrix} \sin t \\ \cos t \end{bmatrix} = \begin{bmatrix} 0 \\ y_c \end{bmatrix} \quad (7)$$

We can solve for the parameter vector $\begin{bmatrix} \sin t & \cos t \end{bmatrix}^T$ and use the Pythagorean trigonometric identity $(\begin{bmatrix} \sin t & \cos t \end{bmatrix}\begin{bmatrix} \sin t & \cos t \end{bmatrix}^T = 1)$ to relate the center coordinate to all other parameters

$$y_c^2 = a^2\sin^2\varphi + b^2\cos^2\varphi \ . \quad (8)$$

Instead of working with the real problem geometry, we rotate and shift our frame of reference such that the major axis is the x-axis and minor axis is the y-axis, see Fig. 4. Thereby we obtain a line connecting the ground coordinates of transmitter and receiver. This line is obtained by transforming the coordinates of the x-axis, i.e., $[x, 0]^T$, via an inverse translation $-\boldsymbol{p}_c$ and an inverse rotation $\boldsymbol{R}_{-\varphi}$. The transformed ground coordinates are given by

$$\begin{bmatrix} x_g \\ y_g \end{bmatrix} = \boldsymbol{R}_{-\varphi}\left(\begin{bmatrix} x \\ 0 \end{bmatrix} - \boldsymbol{p}_c\right) \ . \quad (9)$$

The equation of the transformed ground reads

$$y_g = -x_g\tan\varphi - \frac{y_c}{\cos\varphi} = kx_g - y_0 \quad (10)$$

The ellipse in principal axis is described as $\left(\frac{x}{a}\right)^2 + \left(\frac{y}{b}\right)^2 = 1$. We can solve for negative y and calculate that x coordinate, where its derivative, w.r.t. x, is equal to that of (10).

$$y_{\text{ell}}^{(-)} = -b\sqrt{1-\frac{x^2}{a^2}} \Rightarrow \frac{\partial y_{\text{ell}}^{(-)}}{\partial x} \stackrel{!}{=} k \Rightarrow x_t^2 = \frac{k^2a^4}{b^2+k^2a^2} \quad (11)$$

To let the ellipse touch the ground we have to set y_g and $y_{\text{ell}}^{(-)}$ at x_t equal. We obtain again an equation linking all parameters

$$\frac{(h_t+h_r)^2}{d^2} = \left(\sqrt{\frac{(h_t-h_r)^2+d^2}{d^2}} + \frac{\Phi}{d}\right)^2 \frac{(h_t-h_r)^2}{(h_t-h_r)^2+d^2} + \frac{2\Phi}{d}\sqrt{\frac{d^2}{(h_t-h_r)^2+d^2}} + \left(\frac{\Phi}{d}\right)^2 \frac{d^2}{(h_t-h_r)^2+d^2} \tag{18}$$

$$d_B = \frac{1}{2\Phi}\sqrt{16h_t^2h_r^2 - 4\Phi^2\left(h_t^2+h_r^2\right)+\Phi^4}\,, \quad \text{for } \Phi = \frac{\lambda}{2},\ \left(\frac{\lambda}{2}\right)^2 \ll \left(\min\left\{h_t,h_r\right\}\right)^2 \leq \frac{4h_t^2h_r^2}{\left(h_t+h_r\right)^2} \quad \Rightarrow\ d_B \approx \frac{4}{\lambda}h_th_r \tag{19}$$

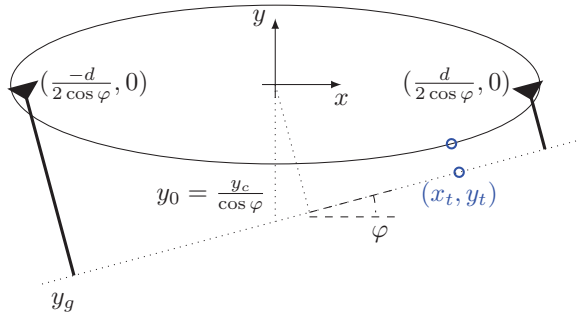

Fig. 4: Ellipse geometry after principal axis transformation.

involved.

$$\frac{k^2a^2}{\sqrt{b^2+k^2a^2}} - y_0 \stackrel{!}{=} \frac{-b^2}{\sqrt{b^2+k^2a^2}} \Rightarrow b^2+k^2a^2 = y_0^2 \tag{12}$$

$$b^2 + a^2\tan^2\varphi = \frac{y_c^2}{\cos^2\varphi} \tag{13}$$

Equation (13) reproduces (8). Transforming our problem into the principal axis form comes with further insights. Assume that vehicles with equal antenna heights are communicating while driving uphill, the antenna of the further up car appears at a lower equivalent flat earth height. It appears as in Fig. 4.

B. When does the first Fresnel zone touch the ground?

Equation (8) gives a relation between the semi-major axis a the semi-minor axis b, the inclination angle φ and the y-coordinate of the center point. The first Fresnel zone gives a specific ellipse, fixing the relationship of a, b and the phase shift at the reflection.

For the first Fresnel zone, the difference in path length between the LOS signal and a reflected signal is half wavelength ($\lambda/2 \triangleq 180°$). Implicitly this assumes that the reflection adds another $180°$ ($\lambda/2$) of phase shift, thereby summing both rays constructively — in phase. Generalizing this concept, we have to enforce that both additional phases (longer path and reflection) need to sum up to $\lambda \triangleq 360°$. Thus, defining Φ as the complimentary phase (in wavelength) to the reflection phase, we can define the semi-major axis as

$$l_{\text{LOS}} + \Phi = 2a\ , \tag{14}$$

Through this relation, b can be expressed as

$$b = \sqrt{a^2 - \left(l_{\text{LOS}}/2\right)^2} = \sqrt{l_{\text{LOS}}\Phi/2 + \Phi^2/4} \tag{15}$$

At first we notice, that the relation between transmitter and receiver ground distance d and LOS distance l_{LOS} defines us $\cos\varphi$ and $\sin\varphi$

$$\cos^2\varphi = \left(\frac{d}{l_{\text{LOS}}}\right)^2 = \frac{d^2}{(h_t-h_r)^2+d^2} \tag{16}$$

$$\sin^2\varphi = 1-\cos^2\varphi = \frac{(h_t-h_r)^2}{(h_t-h_r)^2+d^2} \tag{17}$$

Putting Equations (14)-(17) into (8) and dividing by d^2 leads to Equation (18). Solving Eq. (18) for d gives the break point distance in (19)[1]. The authors of [1], [2] provide the equivalent solution for the special case of $\Phi = \lambda/2$, but without derivation.

C. Relationship between First Fresnel Zone and 2R Model

To understand the relation between the 2R model and the first Fresnel Zone, we work with the idealistic assumptions leading to Equation (4). For these assumptions the break point can be very well approximated as $d_B = 4h_th_r/\lambda$. Evaluating the argument of the sine term in (4) gives $\pi/2$, which is the first local maximum of a sine wave. Figure 5 marks this point. Putting it more precisely, the first Fresnel zone describes the last inflection point of the receive power and afterwards the decrease of the receive power is stronger than the quadratic envelope; the dotted red line.

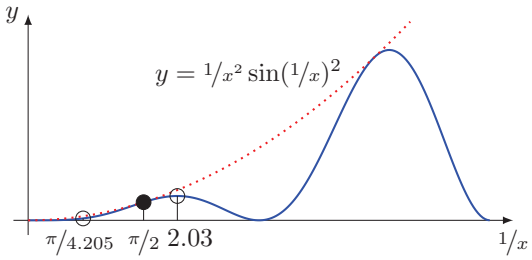

Fig. 5: Simplified oscillatory power as function plotted in reciprocal distance. The first blank circle (from left) marks the proposed break point distance in [17]. The filled circle — an inflection point — corresponds to the break point distance derived from the first Fresnel zone. The last (blank) circle is the local maximum at maximum distance.

In most mmWave scenarios, see Table I, d_B is at very large distances. Due to receiver sensitivity, d_B will hardly be observable with mmWave equipment. For car-to-car scenarios, where the transceiver is in the bumper of the car (possibly collocated to the radar equipment), the break point distance is observable, see bold faced entry in Table I.

IV. Finding the Break Point

The 2R model has its widespread use for modelling the path loss coefficient in wireless communications systems. Until the break point, LOS propagation with path loss coefficient of $n = 2$ is used, and above the break point the path loss

[1]The solution (19) for $h_t, h_r, \lambda > 0$ was calculated using the computer algebra system SymPy.

	f_0 in GHz	h_t in m	h_r in m	d_B in m
Car-to-Car	5.9	1.5	1.5	177
	60	1.5	1.5	1800
	60	0.5	0.5	**200**
Train-to-Infrastructure	2.5	10	3	1000
	60	10	3	24000
Mobile Communications	2.5	10	1.5	500
	2.5	35	1.5	1750
	60	35	1.5	42000

TABLE I: Break point distances with $\Gamma = -1$.

coefficient is chosen to be $n = 4$. Contrary to this usage, the 2R model is a small scale fading model! Similar to [15], we employ the channel impulse response for our argumentation.

$$h(\tau) = a_{\text{LOS}}\delta(\tau) + a_{\text{R}}\delta(\tau - \tau_0), \quad \tau_0 = \frac{\Delta l}{c}, \tag{18}$$

where a subsumes the antenna gains and distance dependent loss for both paths, respectively. Assuming a relatively long ground distance d we can approximate Equation (18) with

$$h(\tau) \approx \frac{\lambda\sqrt{G^t G^r}}{4\pi d}\left(\delta(\tau) - \delta\left(\tau - \frac{2h_t h_r}{d}\frac{1}{c}\right)\right). \tag{19}$$

In case we can resolve both delays, we could use a multipath receiver, e.g., a rake, and collect the energy of both rays. The received power $\|h(\tau)\|^2$ then falls off quadratically in the distance.

So, what do we observe for example in Fig. 2? It is small scall fading! A (relatively) narrowband receiver cannot resolve both rays individually and adds them up. As the phases vary different for both paths, an interference pattern is caused by the receive filter convolution. Figure 6 shows a scenario for $f_0 = 60\,\text{GHz}$ and $h_t = h_r = 0.5\,\text{m}$.

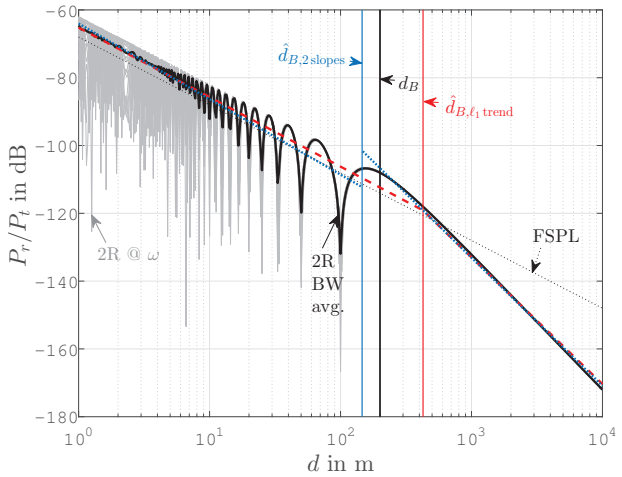

Fig. 6: 2R model with 2R pattern for a single frequency underlaid in grey. The black solid line is a power average over 2 GHz bandwidth. This 2R pattern would we visual in a IEEE 802.11ad system. The black vertical line marks d_B.

From a measurement perspective, ideally, we resolve the interfering rays until the break point distance, thereby we come close to the large scale fading assumption (a simple kink in the path loss slope). On such a measurement data set, the break point can be very accurately obtained.

$$BW \approx {}^1\!/_{\tau_0} = {}^{c}\!/_{2h_t h_r} \overset{d=d_B}{=} 2f_0 \tag{20}$$

For UWB frequency ranges, this relative bandwidth of 2 is realizable with state of the art equipment. For mmWaves such extrem bandwiths are not realizable yet.

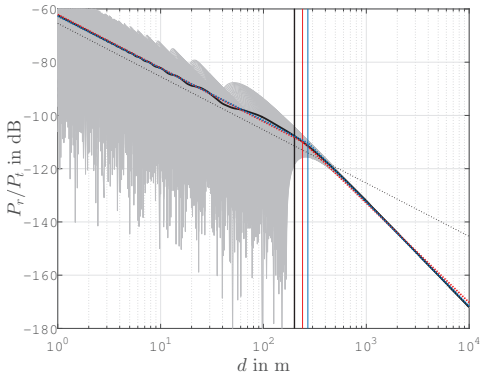

Fig. 7: Same scenario as Fig. 6 with $BW = 80\,\text{GHz}$ average.

A. ℓ_1 Trend Filtering

The problem of finding a piecewise linear trend with the smallest number of kinks, bounding the residual norm is called ℓ_1 trend filtering [16]. The number of kinks is determined via the second-order difference matrix $\boldsymbol{D}$ and can be measured via the zero-pseudo norm of $\boldsymbol{D}\boldsymbol{r}_{\ell_1}$, where $\boldsymbol{r}_{\ell_1}$ is the optimization variable. To relax this problem to a convex one, the zero-norm is replaced by the ℓ_1-norm. The problem in Lagrange form with 2R model observations $\boldsymbol{r}_{2\text{R}}$ reads

$$\min_{\boldsymbol{x}} \|\boldsymbol{r}_{2\text{R}} - \boldsymbol{r}_{\ell_1}\|_2^2 + \mu\,\|\boldsymbol{D}\boldsymbol{r}_{\ell_1}\|_1 \ . \tag{21}$$

Eq. (21) is a generalized LASSO [18]. The regularization parameter μ can be obtained via the solution path from [18] or with the more efficient algorithm proposed in [19], [20]. The minimizer of (21) is shown in red dashed lines in Figs. 6 and 7.

B. Two Slope Fit

We compare the performance of ℓ_1 trend filtering with a grid search algorithm. Therefore we fit a first straight line on the double logarithmic data until the initial guess of the break point. After that break point we fit a second line. We search among various possible break point distances $\hat{d}$, in steps of $0.01^{4h_t h_r}/_{\lambda}$, and chose that one with smallest Mean Squared Error (MSE) — the best fit. The fits are drawn in dotted blue lines in Figs. 6 and 7.

C. Bandwidth Dependent Error

In Figs. 6 and 7, one can clearly observe, that the quality of the break point estimation depends on the measurement bandwidth. In Fig. 8, we sweep over bandwidth to illustrate this behaviour. As claimed, for large enough bandwidths, both algorithms estimate d_B pretty well. The jump in the relative error of the 2 slopes fit comes from the non-convex decision function. In Fig. 9, we plotted the MSE over the search space $\hat{d}$ for increasing bandwidth. After the third increase the shape of the decision function changes and another local minima becomes the global minimum. In contrast, ℓ_1 trend filtering show a continuous trend with bandwidth increase.

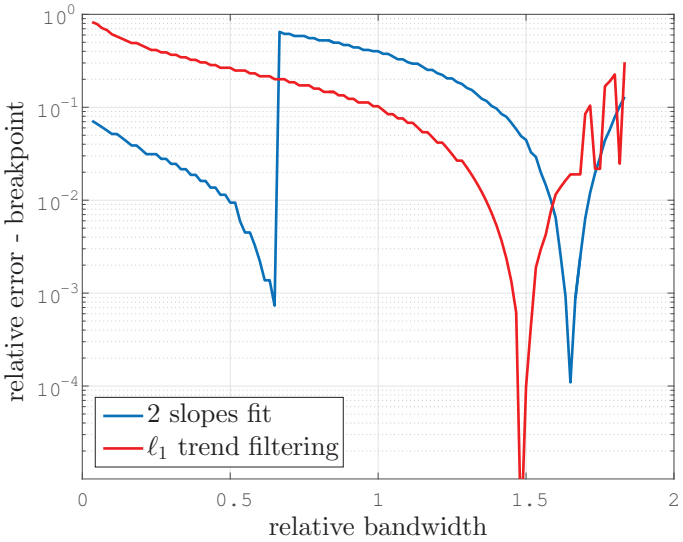

Fig. 8: Relative estimation error $(\hat{d}_B - d_B)^2/d_B^2$ for the break point as function of relative bandwidth BW/f_0.

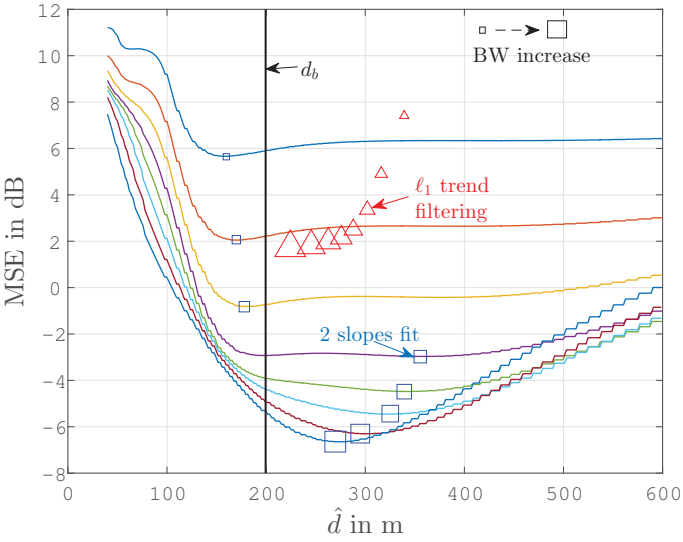

Fig. 9: Non-convex decision function for 2 slopes fit.

V. Conclusion

The 2R model has been observed experimentally and through ray-tracing simulations. We derived the break point distance based on (a generalized) first Fresnel zone and showed that the simple approximation formula is still valid. We then focused on estimating this break point and showed that large measurement bandwidths are necessary to estimate the break point distance accurately.

Acknowledgements

The financial support by the Austrian Federal Ministry of Science, Research and Economy and the National Foundation for Research, Technology and Development is gratefully acknowledged. The research has been co-financed by the Czech Science Foundation, Project No. 17-18675S "Future transceiver techniques for the society in motion", and by the Czech Ministry of Education in the frame of the National Sustainability Program under grant LO1401.

References

[1] H. Xia, H. L. Bertoni, L. R. Maciel, A. Lindsay-Stewart, and R. Rowe, "Radio propagation characteristics for line-of-sight microcellular and personal communications," *IEEE Transactions on Antennas and Propagation*, vol. 41, no. 10, pp. 1439–1447, 1993.

[2] M. J. Feuerstein, K. L. Blackard, T. S. Rappaport, S. Y. Seidel, and H. H. Xia, "Path loss, delay spread, and outage models as functions of antenna height for microcellular system design," *IEEE Transactions on Vehicular Technology*, vol. 43, no. 3, pp. 487–498, 1994.

[3] E. Zöchmann, M. Lerch, S. Caban, R. Langwieser, C. F. Mecklenbräuker, and M. Rupp, "Directional evaluation of receive power, Rician K-factor and RMS delay spread obtained from power measurements of 60 GHz indoor channels," in *Proc. of IEEE-APS Topical Conference on Antennas and Propagation in Wireless Communications (APWC)*, Cairns, Australia, Sep. 2016.

[4] C. Sommer, S. Joerer, and F. Dressler, "On the applicability of two-ray path loss models for vehicular network simulation," in *Proc. of IEEE Vehicular Networking Conference (VNC)*, 2012, pp. 64–69.

[5] J. Karedal, N. Czink, A. Paier, F. Tufvesson, and A. F. Molisch, "Path loss modeling for vehicle-to-vehicle communications," *IEEE Transactions on Vehicular Technology*, vol. 60, no. 1, pp. 323–328, 2011.

[6] J. Kunisch and J. Pamp, "Wideband car-to-car radio channel measurements and model at 5.9 GHz," in *Proc. of IEEE Vehicular Technology Conference (VTC-Fall)*, 2008, pp. 1–5.

[7] P. Liu, D. W. Matolak, B. Ai, and R. Sun, "Path loss modeling for vehicle-to-vehicle communication on a slope," *IEEE Transactions on Vehicular Technology*, vol. 63, no. 6, pp. 2954–2958, 2014.

[8] V. Va, T. Shimizu, G. Bansal, and R. W. Heath Jr, "Millimeter wave vehicular communications: A survey," *Foundations and Trends® in Networking*, vol. 10, no. 1, pp. 1–113, 2016.

[9] N. Fujimoto and M. Nakagawa, "System performance of DS/SS inter-vehicle communication and ranging system under Rician fading channel," in *Proc. of IEEE International Symposium on Personal, Indoor and Mobile Radio Communications (PIMRC)*, 1998, pp. 476–480.

[10] A. Yamamoto, K. Ogawa, T. Horimatsu, K. Sato, and M. Fujise, "Effect of road undulation on the propagation characteristics of inter-vehicle communications in the 60 GHz band," in *Proc. of IEEE/ACES International Conference on Wireless Communications and Applied Computational Electromagnetics*, 2005, pp. 841–844.

[11] H. Meinel and A. Plattner, "Millimetre-wave propagation along railway lines," *IEE Proceedings F (Communications, Radar and Signal Processing)*, vol. 130, no. 7, pp. 688–694, 1983.

[12] K. Guan, G. Li, T. Kürner, A. F. Molisch, B. Peng, R. He, B. Hui, J. Kim, and Z. Zhong, "On millimeter wave and THz mobile radio channel for smart rail mobility," *IEEE Transactions on Vehicular Technology*, vol. PP, no. 99, pp. 1–1, 2016.

[13] A. Karttunen, C. Gustafson, A. F. Molisch, R. Wang, S. Hur, J. Zhang, and J. Park, "Path loss models with distance-dependent weighted fitting and estimation of censored path loss data," *IET Microwaves, Antennas & Propagation*, vol. 10, no. 14, pp. 1467–1474, 2016.

[14] Y. Chang, S. Baek, S. Hur, Y. Mok, and Y. Lee, "A novel dual-slope mm-Wave channel model based on 3D ray-tracing in urban environments," in *Proc. of IEEE International Symposium on Personal, Indoor, and Mobile Radio Communication (PIMRC)*, 2014, pp. 222–226.

[15] M. Peter, W. Keusgen, and R. J. Weiler, "On path loss measurement and modeling for millimeter-wave 5G," in *Proc. of IEEE European Conference on Antennas and Propagation (EuCAP)*, 2015, pp. 1–5.

[16] S.-J. Kim, K. Koh, S. Boyd, and D. Gorinevsky, "ℓ_1 trend filtering," *SIAM review*, vol. 51, no. 2, pp. 339–360, 2009.

[17] S. Perera, A. Williamson, and G. Rowe, "Prediction of breakpoint distance in microcellular environments," *Electronics Letters*, vol. 35, no. 14, pp. 1135–1136, 1999.

[18] R. J. Tibshirani and J. Taylor, "The solution path of the generalized LASSO," *The Annals of Statistics*, vol. 39, no. 3, pp. 1335–1371, 2011.

[19] C. F. Mecklenbräuker, P. Gerstoft, and E. Zöchmann, "c–LASSO and its dual for sparse signal estimation from array data," *Signal Processing*, vol. 130, pp. 204–216, 2017.

[20] E. Zöchmann, P. Gerstoft, and C. F. Mecklenbräuker, "Density evolution of sparse source signals," in *Proc. of International Workshop on Compressed Sensing Theory and its Applications to Radar, Sonar and Remote Sensing (CoSeRa)*. IEEE, 2015, pp. 124–128.